J|A|C|S
ARTICLES
Published on Web 09/27/2006

Proline Zwitterion Dynamics in Solution, Glass, and Crystalline State

Josef Kapitán,[†,‡] Vladimír Baumruk,[‡] Vladimír Kopecký, Jr.,[‡] Radek Pohl,[†] and Petr Bouř*[,†]

Contribution from the Institute of Organic Chemistry and Biochemistry, Academy of Sciences, Flemingovo nám. 2, 16610, Prague 6, Czech Republic, and Charles University, Faculty of Mathematics and Physics, Institute of Physics, Ke Karlovu 5, 12116, Prague 2, Czech Republic

Received April 28, 2006; E-mail: bour@uochb.cas.cz

Abstract: Raman and Raman optical activity spectra of L- and D-proline zwitterionic (PROZW) forms were recorded for H_2O and D_2O solutions in a wide frequency range and analyzed with respect to the motion of the proline ring and rotation of the carbonyl group. The solution spectra were additionally compared to Raman scattering of glass and crystalline powder proline. Solution and glass spectral band broadenings are similar and reveal information about the extent of internal molecular motion. Two distinct but equally populated flexible forms were found in the glass and the solution. The equal population is consistent with NMR data, temperature, and concentration dependencies. The molecular flexibility is reduced significantly in the crystal, however, where only one conformer is present. Consequently, the crystal bands are narrow and exhibit minor frequency shifts. The spectra were interpreted with the aid of density functional theory computations involving both continuum and explicit solvent. A two-dimensional potential energy surface pertaining to the five-member ring puckering coordinates was constructed and used for dynamical averaging of spectral properties. Comparison of the computed and experimental bandwidths suggests that the puckering is strongly correlated with the carbonyl rotation. An averaging over these two motions produces similar results. The interpretation of the Raman experiments with the aid of the simulation techniques also indicates that the environment modulates properties of the hydrophobic part of the molecule indirectly by interacting with the ionic group. Such behavior may be important for the reactivity and biological activity of proline-containing peptides and proteins.

Introduction

It is now generally accepted that not only structure but also flexibility is important for the reactivity and biological role of many molecules.[1−3] As the dynamical processes are quite complex, it appears convenient to study particular aspects of molecular motions on small, well-defined systems that can be understood in detail. In the past, we and others found it useful to improve the methodology of vibrational spectroscopies for conformational studies of simple peptide and protein building blocks.[4−7] Apart from the experimental merits,[8] the fast optical response makes the infrared and Raman techniques especially suitable for monitoring of the relatively slow conformational changes. The nuclear magnetic resonance (NMR) data are valuable as well, but usually pertain to an average geometry only.[9] Nevertheless, as the vibrational spectral shapes are usually determined by an equilibrium predominant structure, the detection and interpretation of the dispersion changes caused by molecular motion are difficult. Quite often spectral bands are broadened by the inseparable influence of the conformational equilibria, temperature motions, and solvent−solute interactions.[10,11] On the other hand, when the effects of the structural fluctuations on the spectra can be assessed, for example, for the Raman scattering of alanine,[12] better agreement between experiment and simulation and valuable information about the molecular potential energy surface can be obtained. Therefore, in this study, we focus on the detection of proline flexibility in different phase states using NMR, Raman, and Raman optical activity spectroscopies. Supposedly, the complex approach better

[†] Academy of Sciences.
[‡] Charles University.

(1) Peterson, J. R.; Bickford, L. C.; Morgan, D.; Kim, A. S.; Ouerfelli, O.; Kirschner, M. W.; Rosen, M. K. *Nat. Struct. Mol. Biol.* **2004**, *11*, 747−755.
(2) Plaxco, K. W.; Gross, M. *Nature* **1997**, *386*, 657−659.
(3) Uversky, V. N. *Proteins* **2000**, *41*, 415−427.
(4) Jalkanen, K. J.; Elstner, M.; Suhai, S. *THEOCHEM* **2004**, *675*, 61−77.
(5) Jalkanen, K. J.; Nieminen, R. M.; Knapp-Mohammady, M.; Suhai, S. *Int. J. Quantum Chem.* **2003**, *92*, 239−259.
(6) Eker, F.; Cao, X.; Nafie, L.; Schweitzer-Stenner, R. *J. Am. Chem. Soc.* **2002**, *124*, 14330−14341.
(7) Bouř, P.; Buděšínský, M.; Špirko, V.; Kapitán, J.; Šebestík, J.; Sychrovský, V. *J. Am. Chem. Soc.* **2005**, *127*, 17079−17089.
(8) Keiderling, T. A.; Silva, R. A. G. D. Conformational studies using infrared techniques. In *Synthesis of peptides and peptidomimetics*; Goodman, M., Felix, A., Moroder, L., Toniolo, C., Eds.; Georg Thieme Verlag: Stuttgart, 2002; Vol. E22b.
(9) Evans, J. N. S. *Biomolecular NMR Spectroscopy*; Oxford University Press: Oxford, 1995.
(10) Bouř, P.; Keiderling, T. A. *J. Phys. Chem. B* **2005**, *109*, 23687−23697.
(11) Yang, S.; Cho, M. *J. Chem. Phys.* **2005**, *123*, 134503.
(12) Kapitán, J.; Baumruk, V.; Kopecký, V., Jr.; Bouř, P. *J. Phys. Chem. A* **2006**, *110*, 4689−4696.

explores the potential of individual techniques and brings further understanding of the behavior of this important peptide building block. Especially, the gel-like glass form of proline that could be obtained by the relatively novel technique of the drop coating deposition Raman spectroscopy[12−14] nicely complements the knowledge about the physical properties of this amino acid.

Proline is an essential part of most peptides and proteins where it can modulate the structure and biological function.[15] It is the primary building block of collagen. The enhancement of the peptide chain turning in β-sheet structures is another typical example of the importance of its conformational flexibility.[16] Furthemore, it has been shown that toxicity of proline derivatives may be dependent on the ring conformation.[17] The proline zwitterion (PROZW) itself thus represents a convenient experimental and theoretical model system for analyzing the behavior of the proline residue. Previous theoretical and experimental studies indicate that two distinct equally populated PROZW conformers exist in solution,[18] while one or the other is present in the solid state, according to the crystal type.[19,20] Mixed conformations are possible in peptides and proteins.[21] However, the flexible pyrrolidine ring is significantly influenced by the environment, and the puckering is dependent on conformations of attached residues if the ring is blocked or built in peptides.[22−24] For example, theoretical analysis confirmed a correlation with the *cis*−*trans* amide bond isomerization in Ac−Pro−NHMe.[25] An approximate 1:1 ratio for the proline ring conformers is suggested for aqueous polyproline solutions in our latest analysis of their Raman and Raman optical activity spectra.[26] In collagen, a significant slowing of the ring motion was found for hydroxyproline as compared to sole proline by solid-state NMR.[27] Final conformation properties of the proline ring can be tuned not only by the peptide chain lengthening but also by substitutions on the aliphatic part, as was explored for the 4-substituted derivatives.[28]

Historically, charged proline forms[29] or neutral derivatives[25,30,31] were studied more often than the zwitterion, because the latter form is not stable in a vacuum and many computational methods could not be applied.[32,33] For neutral proline vibrational normal modes have been classified, too.[34] A description of the larger-amplitude motion of the five-member ring based on conventional torsion angles was found difficult because of the cyclic constraint.[25,30] Typically, a hysteretic dependence of the energy on the angle was obtained. Additionally, coupling of the ring and side group movements was suggested.[31] To avoid these difficulties we performed a full two-dimensional (2D) scan of the molecular energy surface using the pseudorotation ring puckering coordinates.[35,36] The original definition of the puckering coordinates,[35,37] most common in saccharide chemistry, was found satisfactory here, exhibiting only minor practical differences if compared with the more general definition of Cremer and Pople.[38] The theoretical analysis has been enabled by the latest development of computational tools. Particularly, a semianalytical implementation of the computation of the Raman intensity tensors and harmonic force field within the density functional theory (DFT) enabled relatively fast spectra generation for multiple PROZW structures.[39−41] The aqueous PROZW environment was simulated with explicit water molecules as well as using the continuum COSMO reaction field.[42,43] We would like to emphasize that a high precision in the computation of vibrational frequencies is required for reproduction of the fine mode splitting determining the ROA intensities, which could not be achieved with available implementations of such models until recently.

Raman spectroscopy is one of the few methods that enable monitoring of behavior of biologically relevant molecules in an aqueous environment.[44,45] Its extension, the Raman optical activity (ROA), measures the scattering differences between left- and right-circularly polarized light and is more sensitive to detailed molecular structure and conformation.[46−51] With our ROA instrument[52−54] we could thus obtain a signal covering most of the fundamental frequencies with the enhanced structural

(13) Deegan, R. D.; Bakajin, O.; Dupont, T. F.; Huber, G.; Nagel, S. R.; Witten, T. A. *Nature* **1997**, *389*, 827−829.
(14) Zhang, D.; Mrozek, M. F.; Xie, Y.; Ben-Amotz, D. *Appl. Spectrosc.* **2004**, *58*, 929−933.
(15) Feng, Y. Q.; Klein, B. K.; Vu, L.; Aykent, S.; McWherter, C. A. *Biochemistry* **1995**, *34*, 6540−6551.
(16) Yao, J.; Dyson, H. J.; Wright, P. E. *J. Mol. Biol.* **1994**, *243*, 754−766.
(17) Falk, M.; Sidhu, P.; Walter, J. A. *Nat. Toxins* **1998**, *6*, 159−171.
(18) Haasnoot, C. A. G.; DeLeeuw, F. A. A. M.; DeLeeuw, H. P. M.; Altona, C. *Biopolymers* **1981**, *20*, 1211−1245.
(19) Sarkar, K.; Young, P. E.; Torchia, D. A. *J. Am. Chem. Soc.* **1986**, *108*, 6459−6464.
(20) Kayushina, R. L.; Vainshtein, B. K. *Kristallografiya (Crystallogr. Rep.)* **1965**, *10*, 833−844.
(21) Madi, Z. L.; Griesinger, C.; Ernst, R. R. *J. Am. Chem. Soc.* **1990**, *112*, 2908−2914.
(22) Pal, D.; Chakrabarti, P. *J. Mol. Biol.* **1999**, *294*, 271−288.
(23) White, E. J. M.; Bell, L. H.; Maccallum, P. H. *J. Mol. Biol.* **1992**, *228*, 725−734.
(24) Vitagliano, L.; Berisio, R.; Mastrangelo, A.; Mazzarella, L.; Zagari, A. *Protein Sci.* **2006**, *10*, 2627−2632.
(25) Kang, Y. K.; Choi, H. Y. *Biophys. Chem.* **2004**, *11*, 135−142.
(26) Kapitán, J.; Baumruk, V.; Kopecký, V., Jr.; Bouř, P. *J. Am. Chem. Soc.* **2006**, *128*, 2438−2443.
(27) Reichert, D.; Pascui, O.; deAzevedo, E. R.; Bonagamba, T. J.; Arnold, K.; Huster, D. *Magn. Reson. Chem.* **2004**, *42*, 276−284.
(28) Song, I. K.; Kang, Y. K. *J. Phys. Chem. B* **2005**, *109*, 16982−16987.
(29) Pecul, M.; Ruud, K.; Rizzo, A.; Helgaker, T. *J. Phys. Chem. A* **2004**, *108*, 4269−4276.
(30) Kang, Y. K. *J. Phys. Chem. B* **2004**, *108*, 5463−5465.
(31) Ramek, M.; Kelterer, A. M.; Nikolic, S. *Int. J. Quantum Chem.* **1997**, *65*, 1033−1045.
(32) Czinki, E.; Csaszar, A. G. *Chem.—Eur. J.* **2003**, *9*, 1008−1019.
(33) Allen, W. D.; Czinki, E.; Császár, G. A. *Chem.—Eur. J.* **2004**, *10*, 4512−4517.
(34) Tarakeshwar, P.; Manogaran, S. *THEOCHEM* **1996**, *365*, 167−181.
(35) Altona, C.; Sundaralingam, M. *J. Am. Chem. Soc.* **1972**, *94*, 8205−8212.
(36) Harvey, S. C.; Prabhakaran, M. *J. Am. Chem. Soc.* **1986**, *108*, 6128−6136.
(37) DeTar, D. F.; Luthra, N. P. *J. Am. Chem. Soc.* **1977**, *99*, 1232−1244.
(38) Cremer, D.; Pople, J. A. *J. Am. Chem. Soc.* **1975**, *97*, 1354−1358.
(39) Frisch, M. J., et al. *Gaussian 03*, revision C.02; Gaussian, Inc.: Wallingford, CT, 2004.
(40) Ruud, K.; Helgaker, T.; Bouř, P. *J. Phys. Chem. A* **2002**, *106*, 7448−7455.
(41) Angeli, C., et al. *Dalton, a molecular electronic structure program*, Release 2.0; University of Oslo: Oslo, 2005.
(42) Klamt, A.; Schuurmann, G. *J. Chem. Soc., Perkin Trans.* **1993**, *2*, 799−805.
(43) Klamt, A. COSMO and COSMO-RS. In *The Encyclopedia of Computational Chemistry*; Schleyer, P. R., Allinger, N. L., Clark, T., Gasteiger, J., Kollman, P. A., Schaefer, H. F., III, Schreiner, P. R., Eds.; John Wiley & Sons: Chichester, 1998; Vol. 1, pp 604−615.
(44) Williams, R. W. *Methods Enzymol.* **1986**, *130*, 311−331.
(45) Bussian, B. M.; Sander, C. *Biochemistry* **1989**, *28*, 4271−4277.
(46) Barron, L. D.; Hecht, L.; Bell, A. D. Vibrational Raman Optical Activity of Biomolecules. In *Circular Dichroism and the Conformational Analysis of Biomolecules*; Fasman, G. D., Ed.; Plenum: New York, 1996; pp 653−695.
(47) McColl, I. H.; Blanch, E. W.; Hecht, L.; Kallenbach, N. R.; Barron, L. D. *J. Am. Chem. Soc.* **2004**, *126*, 5076−5077.
(48) Barron, L. D.; Hecht, L.; McColl, I. H.; Blanch, E. W. *Mol. Phys.* **2004**, *102*, 731−744.
(49) Nafie, L. A.; Freedman, T. B. Vibrational optical activity theory. In *Circular Dichroism. Principles and Applications*, 2nd ed.; Berova, N., Nakanishi, K., Woody, R. W., Eds.; Wiley-VCH: New York, 2000.
(50) Tam, C. N.; Bouř, P.; Keiderling, T. A. *J. Am. Chem. Soc.* **1997**, *119*, 7061−7064.
(51) McColl, I. H.; Blanch, E. W.; Gill, A. C.; Rhie, A. G. O.; Ritchie, M. A.; Hecht, L.; Nielsen, K.; Barron, L. D. *J. Am. Chem. Soc.* **2003**, *125*, 10019−10026.
(52) Kapitán, J.; Baumruk, V.; Gut, V.; Hlaváček, J.; Dlouhá, H.; Urbanová, M.; Wunsch, E.; Maloň, P. *Collect. Czech. Chem. Commun.* **2005**, *70*, 403−409.
(53) Bouř, P.; Kapitán, J.; Baumruk, V. *J. Phys. Chem. A* **2001**, *105*, 6362−6368.

information. Although ROA spectra of simple amino acids and peptides have been reported,[6,53,55−58] an ROA signal of the proline zwitterion has never been analyzed before. Estimation of the influences of the solvent and molecular flexibility on the spectra, necessary for PROZW, also appear important to the development of ROA spectroscopy.[59,60] Finally, as a detailed PROZW conformational analysis of Haasnoot and others[18] was based on NMR data, we also find it useful to relate the Raman and ROA spectra to NMR.

Method

Experiment. The backscattered Raman and incident circular polarization (ICP) ROA spectra of both L- and D-proline enantiomers were recorded on our spectrometer described elsewhere.[52,54] Both enantiomers were purchased from Sigma and used without further purification. Water (H_2O) solutions with final concentrations of about 3 mol/L were prepared with deionized water; D_2O solutions (2 mol/L) were prepared from doubly lyophilized samples. The laser excitation wavelength was 514.5 nm, with a laser power of 440 mW, a spectral resolution of 6.5 cm^{-1}, and acquisition times of 6 and 9 h for the H_2O and D_2O measurements, respectively.

The solution Raman PROZW spectra were remeasured together with those of the crystalline and glass samples on the LabRam HR800 Raman microspectrometer (Horiba Jobin Yvon). A continuous Kiefer scanning mode was used with a 600 grooves/mm grating, a liquid-nitrogen cooled CCD detector (1024 × 256 pixels), a spectral resolution of about 4 cm^{-1} (varying within the spectral range of frequencies recorded simultaneously), and a 632.8 nm laser excitation wavelength. For the crystalline sample, a microscope objective of a moderate magnification (10×) was used to focus 20 mW of excitation laser power to a 2 μm diameter spot on the powder sample, and the spectrum was integrated for 4 min. Signals of variously diluted solutions (1, 2, 3, 4, 5, and 6 M) were detected in a macro-mode with 20 mW laser power at the sample and 4 min of integration time. The glass form of PROZW was prepared by deposition and evaporation of 4 μL of 0.01 mg/mL L-proline solution on a standard drop coating deposition Raman (DCDR) substrate SpectRIM (Tienta Sciences). The substrate consisted of a polished stainless steel plate coated with a thin hydrophobic Teflon layer.[13,14,61] The drop was allowed to dry for 20 min at room temperature, and the spectrum was collected with a 100× microscope objective, 2 mW of laser power, and an integration time of 50 min. It is important to note that highly diluted solutions are required at the start to achieve the nonequilibrium nonhomogeneous conditions needed for the glass formation during the evaporation. From more concentrated solutions the amino acid precipitates in the crystalline state.

D_2O solution ^1H NMR spectra of L-proline were recorded on a Bruker Avance spectrometer with a frequency of 500 MHz, with 1,4-dioxane as internal standard,[62] at concentrations of 1 mM, 1 M, and 6 M, and at room temperature (~20 °C). For the 1 mM solution, the measurement was repeated for temperatures of 30, 60, and 90 °C. Indirect nuclear spin−spin coupling constants were obtained by the combination of a first-order multiplet analysis with a simulation of the spectrum using the NMR-Sim 4.3 software. Conformation analysis was performed using program PSEUROT 6.3[63] suited specially for analysis of five-membered rings. Default PSEUROT ring parametrization including relationships between endo- and exo-cyclic torsion angles and group electronegativities was used.

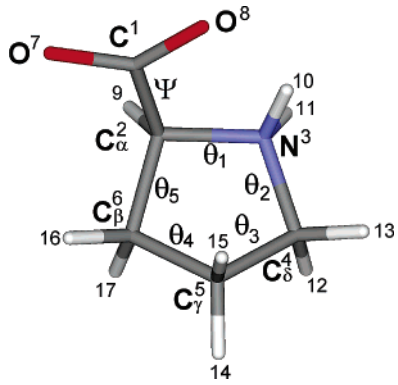

Figure 1. Atom numbering and characteristic torsion angles (ψ(3, 2, 1, 8), θ_1(6, 2, 3, 4), θ_2(2, 3, 4, 5), θ_3(3, 4, 5, 6), θ_4(4, 5, 6, 2), θ_5(5, 6, 2, 3)) in PROZW.

Calculations. Equilibrium geometries, the molecular potential energy surface (PES), and harmonic force fields were computed with the Gaussian program[39] at the B3LYP[64]/COSMO[43]/6-31++G** level. Additionally, HF, MP2, and other DFT functionals were used for control computations. The default grid with 75 radial and 302 angular points was used in the numerical integral estimations. Unconstrained coordinates were always allowed to relax fully. Automatic transition-state localization and a minimum-energy path search[65,66] implemented in Gaussian were explored. Apart from the torsion angles ψ, θ_1...θ_5 defined in Figure 1 the geometry of the five-membered ring was also characterized by puckering phase P,

$$\tan(P) = \frac{\theta_3 + \theta_5 - \theta_2 - \theta_4}{2\theta_1[\sin(\pi/5) + \sin(2\pi/5)]}$$

and amplitude θ_m

$$\theta_m = \theta_1/\cos(P)$$

Note that a backward transformation defined by

$$\theta_j = \theta_m \cos\left(P + \frac{4\pi}{5}(j-1)\right), \qquad j = 1...5$$

is meaningful for ideal rings only.[35,36] Thus the PES scan was based on the torsion angles, particularly with the angle θ_1 incremented within −60°...60° by 2.5°, and for each value of θ_1 the angle θ_2 was scanned using the same step size in a range allowing us to obtain all the ring amplitudes within 0°...60°. Finally, the PES was expressed in the pseudoration coordinates (P, θ_m), and in this representation two-dimensional wave functions and probability distributions were calculated by solving the Schrödinger equation in nonorthogonal coordinates,[67,68] with the aid of a planar wave basis. Final probability distribution was obtained by Boltzmann weighting of all state probabilities.

(54) Bouř, P.; Baumruk, V.; Hanzlíková, J. *Collect. Czech. Chem. Commun.* **1997**, *62*, 1384−1395.
(55) Bouř, P.; Sychrovský, V.; Maloň, P.; Hanzlíková, J.; Baumruk, V.; Pospíšek, J.; Buděšínský, M. *J. Phys. Chem. A* **2002**, *106*, 7321−7327.
(56) Freedman, T. B.; Nafie, L. A.; Keiderling, T. A. *Biopolymers* **1995**, *37*, 265−279.
(57) Yu, G. S.; Freedman, T. B.; Nafie, L. A.; Deng, Z. Y.; Polavarapu, P. L. *J. Phys. Chem.* **1995**, *99*, 835−843.
(58) Zuk, W. M.; Freedman, T. B.; Nafie, L. A. *Biopolymers* **1989**, *28*, 2025−2044.
(59) Barron, L. D.; Ford, S. J.; Bell, A. D.; Wilson, G.; Hecht, L.; Cooper, A. *Faraday Discuss.* **1994**, *99*, 217−232.
(60) McColl, I. H.; Blanch, E. W.; Hecht, L.; Barron, L. D. *J. Am. Chem. Soc.* **2004**, *126*, 8181−8188.
(61) Zhang, D.; Xie, Y.; Mrozek, M. F.; Ortiz, C.; Davisson, V. J.; Ben-Amotz, D. *Anal. Chem.* **2003**, *75*, 5703−5709.
(62) Wishart, D. S.; Bigam, C. G.; Yao, J.; Abildgaard, F.; Dyson, H. J.; Oldfield, E.; Markley, J. L.; Sykes, B. D. *J. Biomol. NMR* **1995**, *6*, 135−140.
(63) van Wijk, J.; Haasnoot, C. A. G.; de Leeuw, F. A. A. M.; Huckriede, B. D.; Westra Hoekzema, A.; Altona, C. *PSEUDOROT 6.3*; Leiden Institute of Chemistry, Leiden University: Leiden, The Netherlands, 1999.
(64) Becke, A. D. *J. Chem. Phys.* **1993**, *98*, 1372−1377.
(65) Ayala, P. Y.; Schlegel, H. B. *J. Chem. Phys.* **1997**, *107*, 375−384.
(66) Peng, C.; Ayala, P. Y.; Schlegel, H. B.; J., F. M. *J. Comput. Chem.* **1996**, *17*, 49−56.
(67) Čejchan, A.; Špirko, V. *J. Mol. Spectrosc.* **2003**, *217*, 142−145.
(68) Podolsky, B. *Phys. Rev.* **1928**, *32*, 812−816.

With Gaussian, nuclear magnetic shielding tensors and spin−spin coupling constants were calculated for equilibrium geometries at the B3LYP/COSMO/6-31++G** level with the default gauge-independent (field-dependent) atomic orbital mechanism.[69] The Raman and ROA polarizability tensors[70,71] were calculated alternatively with the Gaussian and Dalton[41] programs, according to computer availabilities. Spectral intensities were generated by our software[72] enabling a combination of various ab initio parameters (e.g., using the B3LYP/COSMO/6-31++G** force field with HF/6-31++G** optical activity tensors). Thus some spectral parameters could be calculated much faster at a lower approximation level with a minimal loss of accuracy.[40] The polarization model[54,73] allowing us to obtain approximate ROA intensities from electric polarizabilities only was often used for spectra estimations as a faster alternative to full ab initio computations. Spectral shapes were simulated with Lorentzian bands 6.5 cm^{-1} wide (full width at half-height, fwhh). Similarly as for sole PROZW, Raman and ROA intensities were obtained also for its explicit complexes with water molecules. To estimate realistic positions of the waters around the solute, an MD simulation was run using the Tinker software.[74] The zwitterion and the solvent were placed in a periodic cubic box 15.022 Å wide under a pressure of 1 atm, temperature 298 K, adopting the TIP3P water model[75] and Amber99 force field.[76] The PROZW geometry was held constant during the simulations. 26 complexes (13 for each conformation) of the solute and 3−8 hydrogen-bonded waters were arbitrarily selected and subjected to a constrained optimization in normal mode coordinates[77,78] with fixed modes within −100 to 100 cm^{-1}. Thus higher-frequency normal modes of interest could be relaxed with a minimal change of the geometry. Finally, the spectra were generated with the B3LYP/6-31++G** harmonic force field and HF/6-31G (HF/6-31++G** for the proline only) intensity tensors.

Results and Discussion

Potential Energy Surface. In accord with previous studies[18] we found two minima on the PES (Figure 2), referred to as **A** ($\theta_m = 40°$, $P = 94°$, $\psi = -1°$, for the B3LYP/COSMO/6-31++G** computation) and **B** ($\theta_m = 40°$, $P = 276°$, $\psi = -7°$). The torsional angles (θ_1...θ_5) adopt (−3°, −21°, 37°, −39°, and 26°) for **A** and almost "mirror" values of (4°, 21°, −37°, 40°, and −27°) for **B**. This local enantiomeric complementarity, however, will be reflected in the optical activity of the whole molecule only vaguely. Conformer **A** can be well-identified with the crystal structure of pure proline ($\theta_m = 41°$, $P = 109°$, $\psi = -7°$).[20] Although various computational levels give similar shapes of PES, a finer conformer ratio cannot be determined solely on the basis of the theory, as different approximations provide relative energy differences for **A**, **B** within −0.33...2.73 kcal/mol (Table 1s in the Supporting Information). Additionally, we suspect that the continuum solvent model may not be adequate for the description of strong interactions between the solvent and polar groups of the solute. The aqueous environment may smooth out energy differences significantly.[79,80] With these uncertainties the calculations are more or less consistent with the 1:1 conformer ratio indicated by the solution experiment at room temperature. A conformer mixture is also consistent with the shallow PES minima and with the simulated probability distribution for the B3LYP/COSMO/6-31++G** force field plotted at the upper left corner of Figure 2. The computation of the probability distribution via the vibrational functions appeared somewhat superfluous, as obtained conformer probabilities were almost indistinguishable from those based on the Boltzmann factors ($\sim e^{-E/(kT)}$) only. The sensitivity of the predicted conformation of this amino acid on the computational details is illustrated also by the fact that although the equilibrium structure **A** is slightly energetically favored, integration of the probability distribution leads approximately to equal populations of both conformers at 298 K again. Strictly speaking, two conformer classes (**A**, **B**) should be distinguished because of the geometry dispersion; for simplicity, however, we identify each conformer with the closest minimum on PES. Clearly, a planar conformation of the proline ring with a relative energy >4 kcal/mol against the minima is not probable under normal conditions, and the two conformers can flip rather via ring twist and transition states **TS1**, **TS2**. From Figure 2 we can see that the states have similar amplitude as **A**, **B**; for transition states the nitrogen atom thus deviates from an approximate four carbon plane (carbon atoms 2, 6, 5, 4; see Figure 1) to a similar extent as the C^5 atom does from the $C^6C^2N^3C^4$ plane in the equilibrium conformations. Detailed geometries of all the important PES states are listed in the Supporting Information (Table 7s). But these states are weakly populated, too, and cannot be detected. Nevertheless it is interesting that we obtained a similar relative energy for the planar state as was found previously for bare pyrrolidine.[81] Our test computation of the pyrrolidine cation (cf. Figure 3s in SI) is in agreement with previous findings; nevertheless the more important transition states are much lower in energy in pyrrolidine than in PROZW (Table 7s). The geometry of the minima and transition states can also be well-related to the Ac−Pro−NHMe and Ac−Pro−NMe_2 derivatives (Table 7s).[25,30] This corresponds to the fact that primarily the covalent bonds determine the conformational properties; pyrrolidine substitution obviously changes the fine energy profile, although we obtained smaller changes in comparison with those predicted for the Ac−Pro−NHMe derivative calculated at a similar level (HF/6-31+G(d)/CPCM).[25] Additionally, for Ac−Pro−NHMe, somewhat higher transition states (2.5−3.2 kcal/mol) have been computed. [25] Further hindering of the ring motion was also observed for hydroxyproline.[27] On the other hand, the proline ring conformers **A**, **B** seem to be almost equally populated in most peptides and proline-rich amino acids,[23,26] which suggests a limited effect of groups not directly attached to the ring.

Despite the strong mutual coupling of the torsional rotations within the proline ring (angles $\theta_1-\theta_5$), the torsion angles are often used directly in potential energy scans.[25,30,82] This allows us to estimate energy extremes, although hysteretic energy profiles are often obtained due to the ring tension. For PROZW

(69) Wolinski, K.; Hilton, J. F.; Pulay, P. *J. Am. Chem. Soc.* **1990**, *112*, 8251−8260.
(70) Polavarapu, P. L. *Vibrational spectra: principles and applications with emphasis on optical activity*; Elsevier: Amsterdam, 1998; Vol. 85.
(71) Barron, L. D. *Molecular Light Scattering and Optical Activity*; Cambridge University Press: Cambridge, 2004.
(72) Bouř, P.; Sopková, J.; Bednárová, L.; Maloň, P.; Keiderling, T. A. *J. Comput. Chem.* **1997**, *18*, 646−659.
(73) Bouř, P. *J. Comput. Chem.* **2001**, *22*, 426−435.
(74) Ponder, J. W. *Tinker, Software Tools for Molecular Design*, 3.8; Washington University School of Medicine: Saint Louis, MO, 2000.
(75) Jorgensen, W. L.; Chandrasekhar, J.; Madura, J. D. *J. Chem. Phys.* **1983**, *79*, 926−935.
(76) Wang, J.; Cieplak, P.; Kollman, P. A. *J. Comput. Chem.* **2000**, *21*, 1049−1074.
(77) Bouř, P.; Keiderling, T. A. *J. Chem. Phys.* **2002**, *117*, 4126−4132.
(78) Bouř, P. *Collect. Czech. Chem. Commun.* **2005**, *70*, 1315−1340.
(79) Barron, L. D.; Hecht, L.; Wilson, G. *Biochemistry* **1997**, *36*, 13143−13147.
(80) Bouř, P.; Král, V. *Collect. Czech. Chem. Commun.* **2000**, 65, 631−643.
(81) Han, S. J.; Kang, Y. K. *THEOCHEM* **1996**, *369*, 157−165.
(82) Kang, Y. K.; Park, H. S. *THEOCHEM* **2005**, *718*, 17−21.

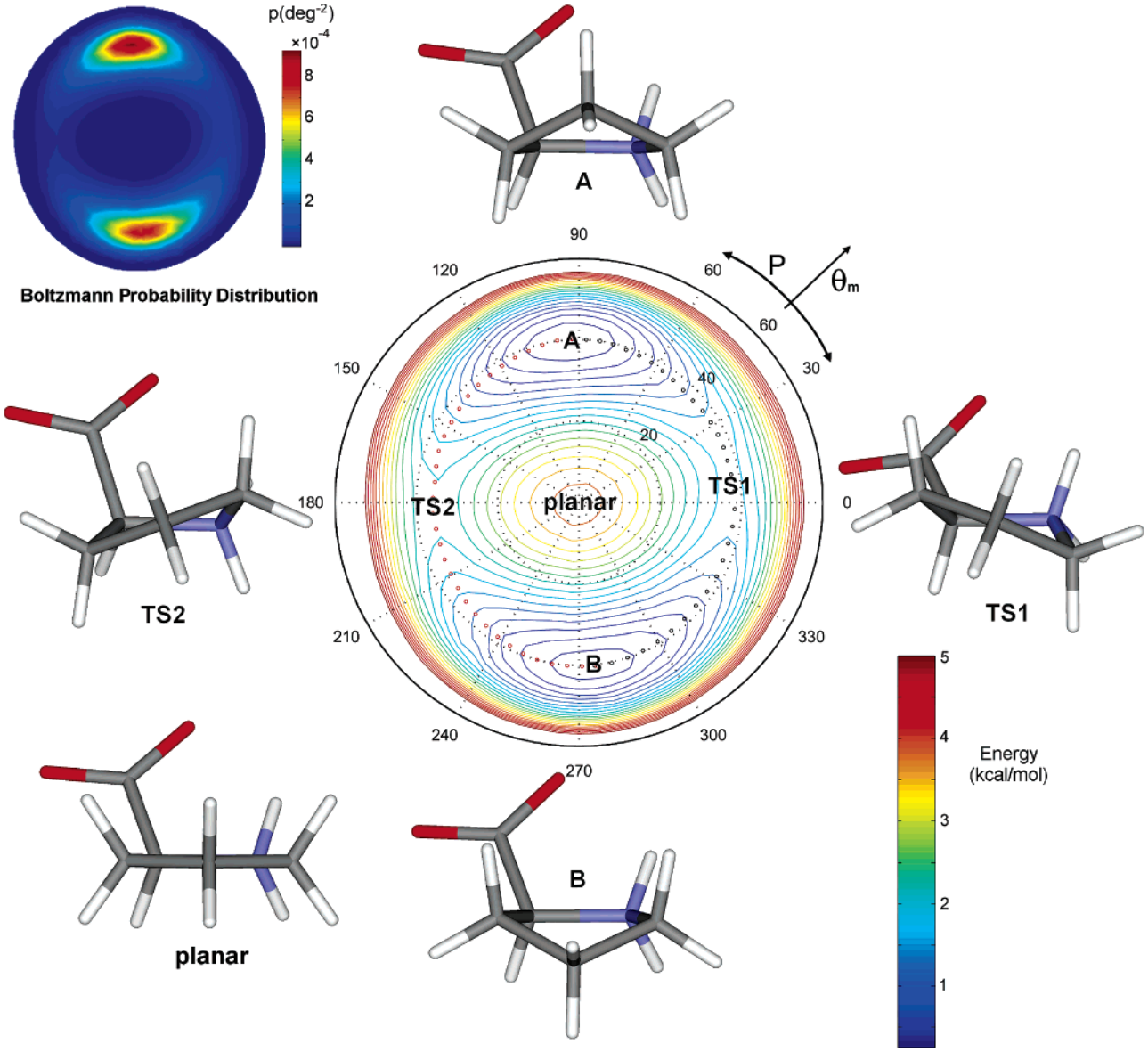

Figure 2. Two-dimensional potential energy surface of PROZW calculated by the B3LYP/6-31++G**/COSMO method and overview of conformer shapes. The ring phase (P) and amplitude (θ_m) are used as polar coordinates; the equipotential lines are spaced by 0.25 kcal/mol. At the upper left corner, the corresponding probability distribution at 300 K is plotted.

an example of such a scan is given in Figure 1s in the Supporting Information. Clearly the constrained torsion scan, even when the remaining coordinates are relaxed, quickly deviates from the energy-minimum path. The latter, however, can be obtained more easily from the pseudorotation phase dependence (Figure 2s).

A 50% fraction of conformer **A** was proposed based on the analysis of NMR data previously.[18] Although our nuclear spin−spin coupling constants slightly differ from the original set, we obtained essentially the same conformer populations, as summarized in Table 1. Nevertheless, the precision of the semiempirical analysis dependent on many ad hoc parameters is limited. For example, the original coupling constant set[83] (second column in the table) provides 60% of the population of conformer **A** if subjected to the standard analysis, while our set (third column) leads to 50%. When the computed spin−spin coupling constants are used in a linear fit (last column in Table 2) a 50% ratio is obtained again, although the computed

Table 1. NMR PROZW Nuclear Spin−Spin Coupling Constants (J, in Hz) and Conformer Populations in D_2O

atoms	J (refs 83,18)	J (this work)	J_{calcd} (**A**, **B**)[a]
9, 17	8.4	8.7	8.7 (10.0, 7.4)
9, 16	6.2	6.2	5.1 (0.6, 9.6)
17, 15	5.6	7.2	6.0 (11.6, 0.3)
17, 14	7.6	7.8	6.1 (6.2, 6.0)
16, 15	7.8	7.9	6.0 (6.3, 5.7)
16, 14	5.6	6.5	5.8 (0.3, 11.2)
15, 12	5.7	7.1	5.8 (11.5, 0.0)
15, 13	7.5	7.1	6.3 (7.0, 5.5)
14, 12	7.9	7.1	6.4 (5.9, 6.9)
14, 13	5.7	7.1	5.8 (0.0, 11.5)
phase[b] (deg, for **A**, **B**)	106, 270	95, 273	94, 276
amplitude (deg, for **A**, **B**)	46, 22	37, 37	40, 40
population of **A** (%)	60	50	50

[a] Average values with constants of the two conformers in parentheses, B3LYP/6-31++G**/COSMO calculation. [b] The phases can be converted to those used in ref 18 by subtracting 108°.

(83) Pogliani, L.; Ellenberger, M.; Valat, J. *Org. Magn. Reson.* **1975**, *7*, 61−71.

Table 2. Calculated and Experimental Frequencies (ω, cm^{-1}) and Normal Mode Assignment of Fundamental Transitions in PROZW

conformer **A**			conformer **B**			ω_{expmtl}[a]		
mode	ω_{calcd}	SAIC(PED)[b]	mode	ω_{calcd}	SIAC(PED)[b]	solution	crystal	glass
1	68	**43**(48) 45(30)	1	65	**43**(51) 45(30)			
2	112	**45**(47) 32(15)	2	110	**45**(50) 32(17)	160 (102)	136	
3	200	**41**(27) 33(26)	3	209	**33**(45)	226 (43)	208 (23)	218
4	280	**33**(31) 39(22)	4	252	**41**(36) 33(15)	295 (76)	299 (15)	280
5	314	**32**(46) 41(21)	5	302	**32**(41) 41(18)	340 (39)	377 (24)	343 (35)
			6	431	**39**(28) 10(15)	442 (36)		449 (38)
6	458	**39**(38)				465 (41)	452 (11)	487 (35)
			7	546	**42**(35)	554 (29)		558 (77)
7	568	**42**(43) 25(15)				578 (50)	578 (11)	558 (77)
8	611	10(17) 38(16)	8	620	**40**(32)	625 (42)	645 (18)	631 (48)
9	658	**40**(48)	9	676	40(28) 38(17)	679 (41)	695 (20)	679 (35)
10	776	**44**(35)	10	764	**44**(41) **38**(21)	781 (28)	795 (13)	780 (26)
11	829	**38**(29) **10**(17)	11	811	**37**(29) 38(17)	846 (24)	845 (10)	846 (26)
12	842	37(22) **21**(20)	12	851	**29**(25) **21**(17)	862 (30)	868 (13)	867 (33)
13	859	**25**(26) **13**(22)	13	857	**25**(24) 17(19)	862 (30)	868 (13)	867 (33)
14	901	**17**(39)	14	903	**17**(36) **16**(25)	907 (26)	902 (8)	904 (22)
15	915	**16**(33) **15**(25)	15	930	**15**(28)	913 (13)	923 (8)	914 (16)
16	942	14(18) 15(15)	16	945	**10**(19)	949 (25)	955 (8)	941 (38)
17	969	**37**(27)	17	978	37(21)	991 (26)	987 (23)	993 (44)
18	1026	17(20) 42(19) 13(15)	18	1029	16(19) 17(18) 42(17)	1036 (19)	1036 (10)	1042 (20)
19	1044	**14**(19)	19	1042	13(14)	1045 (23)	1060 (10)	1057 (23)
20	1093	**29**(21)				1087 (16)	1086 (11)	1091 (27)
			20	1092	**14**(21)	1099 (20)		1091 (27)
21	1164	**36**(24) 30(20) 24(17)	21	1166	**24**(26) **36**(21)	1169 (21)	1167 (12)	1167 (29)
22	1192	**24**(17) **28**(16)	22	1203	**28**(24)	1186 (26)	1178 (10)	1185 (32)
23	1240	35(26) 31(19)	23	1245	**20**(32))	1241 (24)	1241 (13)	1239 (25)
24	1262	36(23) 31(17)	24	1268	24(22) 36(19) 35(17)	1271 (29)	1268 (9)	1268 (29)
25	1291	**30**(31) **20**(17)	25	1294	**27**(24) **30**(24)	1296 (29)	1290 (12)	1298 (48)
26	1324	**27**(47) 23(28)	26	1330	23(25) 30(21) 31(17)	1319 (18)	1321 (17)	1329 (26)
27	1340	11(23) 30(22) 36(20)	27	1339	**31**(28)	1332 (15)		1329 (26)
28	1344	**35**(38) 20(17)	28	1355	**23**(28) 27(19)	1348 (40)		1352 (38)
29	1357	**23**(30) **31**(20)	29	1365	**35**(37)	1348 (40)	1352 (10)	1352 (38)
30	1388	**19**(29) **11**(25)	30	1385	**19**(63)	1398 (45)	1378 (18)	1395 (52)
31	1403	19(26) 11(22)	31	1399	**11**(43) 10(16)	1414 (41)		1415 (46)
32	1488	**22**(67) 26(28)	32	1485	**22**(63) 26(33)	1455 (12)	1444 (12)	1453 (21)
33	1494	**26**(45) 18(40)	33	1491	18(41) **26**(39) 22(17)	1464 (12)	1455 (15)	1461 (20)
34	1504	**18**(54) 26(24) 22(19)	34	1503	**18**(54) 26(25) 22(17)	1478 (15)	1476 (18)	1480 (16)
35	1589	**34**(78)	35	1593	**34**(78)	1571 (87)	1552 (20)	1600 (160)
36	1636	**12**(76)	36	1628	**12**(76)	1620 (59)	1621 (24), 1631 (11), 1652 (7)	1633 (44)
37	3048	**5**(56) 7(18)	37	3043	**7**(46) 5(22) 8(15)	2883(21)	2876 (21)	2855 (18)
38	3055	**7**(39) 5(30) 9(22)	38	3048	**5**(62) 9(17)	2893 (17)	2899 (23)	2883 (26)
39	3060	**9**(69) 7(25)	39	3054	**9**(70) 7(23)	2917 (24)	2933 (18)	2910 (27)
40	3077	**3**(95)	40	3077	**3**(93)	2945 (22)	2950 (18)	2937 (32)
41	3110	**6**(84)	41	3107	**6**(85)	2966 (30)	2971 (12)	2967 (55)
42	3125	**8**(82) 7(15)	42	3121	**8**(81) 7(17)	2996 (44)	2985 (10)	2990 (29)
43	3137	**4**(95)	43	3139	**4**(95)	3003 (21)	3008 (15)	2993 (44)
44	3151	**1**(96)	44	3202	**1**(92)	3031 (27)	3011 (74)	3021 (32)
45	3278	**2**(97)	45	3273	**2**(92)	3057 (143)	3063 (79)	3044 (83)
δ_{av}[b]	4.1			3.6		0	−	
δ_{RMS}[b]	16.8			19.0		0	−	

[a] Bandwidths in parentheses. [b] Symmetry-adapted internal coordinates (SAIC) and their potential energy contributions (in %, for PED > 15%). Bold numbers in the table indicate when a coordinate achieves its maximum PED in the mode. **Definition of SAIC:** (**stretchings:**) **1**(3.10, NH), **2**(3.11, NH), **3**(4.12 + 4.13, $C_\delta H_2$, s), **4**(4.12 − 4.13, $C_\delta H_2$, a), **5**(5.14 + 5.15, $C_\gamma H_2$, s), **6**(5.14 − 5.15, $C_\gamma H_2$, a), **7**(6.16 + 6.17, $C_\beta H_2$, s), **8**(6.16 − 6.17, $C_\beta H_2$, a), **9**(2.9, $C_\alpha H$), **10**(1.2, $C_\alpha C$), **11**(1.7 + 1.8, CO_2^-, s), **12**(1.7 − 1.8, CO_2^-, a), **13**(2.3, $C_\alpha N$), **14**(2.6, $C_\alpha C_\beta$), **15**(5.6, $C_\beta C_\gamma$), **16**(4.5, $C_\gamma C_\delta$), **17**(3.4, $C_\delta N$), (**bendings:**) **18**(3.4.12 + 5.4.12 + 3.4.13 + 5.4.13, $C_\delta H_2$), **19**(3.4.12 − 5.4.12 + 3.4.13 − 5.4.13, $C_\delta H_2$, wagging), **20**(3.4.12 − 5.4.12 − 3.4.13 + 5.4.13, $C_\delta H_2$), **21**(3.4.12 + 5.4.12 − 3.4.13 − 5.4.13, $C_\delta H_2$, rocking), **22**(4.5.14 + 6.5.14 + 4.5.15 + 6.5.15, $C_\gamma H_2$), **23**(4.5.14 − 6.5.14 + 4.5.15 − 6.5.15, $C_\gamma H_2$, wagging), **24**(4.5.14 − 6.5.14 − 4.5.15 + 6.5.15, $C_\gamma H_2$, twisting), **25**(4.5.14 + 6.5.14 − 4.5.15 − 6.5.15, $C_\gamma H_2$, rocking), **26**(5.6.16 + 2.6.16 + 5.6.17 + 2.6.17, $C_\beta H_2$), **27**(5.6.16 − 2.6.16 + 5.6.17 − 2.6.17, $C_\beta H_2$, wagging), **28**(5.6.16 − 2.6.16 − 5.6.17 + 2.6.17, $C_\beta H_2$, twisting), **29**(5.6.16 + 2.6.16 − 5.6.17 − 2.6.17, $C_\beta H_2$, rocking), **30**(6.2.9 + 3.2.9, $C_\alpha H$), **31**(6.2.9 − 3.2.9, $C_\alpha H$), **32**(1.2.6 + 1.2.3, $C_\alpha C$), **33**(1.2.6 − 1.2.3, $C_\alpha C$), **34**(2.3.11 + 4.3.11 + 2.3.10 + 4.3.10, NH_2^+), **35**(2.3.11 − 4.3.11 + 2.3.10 − 4.3.10, NH_2^+, wagging), **36**(2.3.11 − 4.3.11 − 2.3.10 + 4.3.10, NH_2^+, twisting), **37**(2.3.11 + 4.3.11 − 2.3.10 − 4.3.10, NH_2^+, rocking), **38**(2.1.7 + 2.1.8, CO_2^-), **39**(2.1.7 − 2.1.8, CO_2^-), **40**(0.65 × 2.3.4 − 0.51 × (3.2.6 + 3.4.5) + 0.18 × (2.6.5 + 4.5.6), ring bending I), **42**(0.40 × (3.4.5 − 3.2.6) + 0.58 × (2.6.5 − 4.5.6), ring bending II), (**torsions:**) **41**(0.62 × 2.6.5.4 + 0.20 × (4.3.2.6 + 2.3.4.5) − 0.52 × (3.2.6.5 + 3.4.5.6), ring torsion I, puckering), **43**(0.61 × (2.3.4.5 − 4.3.2.6) + 0.36 × (3.2.6.5 − 3.4.5.6), ring torsion II, puckering), **44**(7.1.2.8), **45**(3.2.1.8 + 3.2.1.7 + 6.2.1.8 + 6.2.1.7 + 9.2.1.8 + 9.2.1.7). The atomic numbering is defined in Figure 1; "s" and "a" denote locally symmetrical and asymmetrical combinations. δ_{ave} and δ_{RMS} are average and systematic deviations between experimental and calculated (B3LYP/6-31++G**/COSMO) frequencies; modes 37−45 were not included in the statistics.

values are slightly underestimated on average. Paradoxically, more telling is perhaps the temperature *independence* of the constants (detailed in Table 2s in the Supporting Information). Since no constant changed within the experimental error ($\delta J =$

0.1 Hz), we can estimate the free energy difference from the Boltzmann two-state distribution as

$$\Delta G \cong \frac{4\delta JT}{(J_B - J_A)\Delta T} kT$$

Because the temperature changed by $\Delta T = 70$ K and a maximum of $|J_B - J_A| \approx 10$ Hz, the energy difference must be smaller than 0.1 kcal/mol, and we can set the error bars to the conformer **A** population of (50 ± 4)%. This is in agreement with the theoretical analysis mostly predicting similar energies (within ~1 kcal/mol) for the two conformers (Table 1s in the Supporting Information). Nevertheless it is a pity that available ab initio techniques do not provide more accurate conformer energies in this case. As noticed before[84] the inaccuracy of quantum chemical computations may become a limiting factor even for studies of relatively simple systems and certainly constitutes a challenging task for future development. Clearly, to reliably produce such tiny energy differences, both the level and the implementation of the theory should be improved. With the default Gaussian settings we did not observe troubles with the radial grid for numerical integration (see the test in Table 6s in the Supporting Information), pointed out for similar molecules previously.[85] However, the implementation of the continuum solvent model did exhibit occasional instabilities resulting in convergence difficulties, which could be improved only with a rather tedious change of the model parameters.

Rotation of the CO_2^- group has been largely neglected previously, yet it can perturb the five-member ring geometry significantly. The coupling of these two motions is documented in Figure 3 where dependencies of molecular energy and ring phases on the angle ψ (defined in Figure 1) are plotted for both conformers. Despite the rather high CO_2^- rotational barrier of ~5.5 kcal/mol, rotations within approximately ±15° around the minimum are possible under normal temperature, perturbing thus the ring phases also by about ±15°. A full three-dimensional model involving the puckering and rotational coordinate is currently not feasible; nevertheless, we can estimate the coupling also from the inverse adiabatic 2D dependence of the rotation (ψ) on the ring coordinates (P, θ_m) plotted in Figure 4. For transition states, the angle ψ changes by about ±10° around the equilibrium value, and thus the ring dynamics are presumably controlled to a high extent by the temperature fluctuations of the CO_2^- group position. We note that the PROZW model cannot be directly extended to other proline derivatives, where the ring motion may be restricted by other functional groups to a greater extent.[30,82] However, a similar coupling between the proline ring and a main chain motion as suggested by Figure 4 may be expected also in protein containing peptides.

Vibrational Normal Mode Assignment. Calculated and experimental Raman and ROA spectra of normal (H_2O) and deuterated (D_2O) PROZW solutions are plotted in Figure 5. The frequency region that could be measured encompasses most of the fundamental transitions, and the nearly mirror image of the ROA spectra for D- and L-enantiomers confirms that almost no artifacts are present. Equal populations of the conformers **A** and **B** were assumed for the simulated spectra. The B3LYP/6-31++G**/COSMO level and the harmonic approximation were

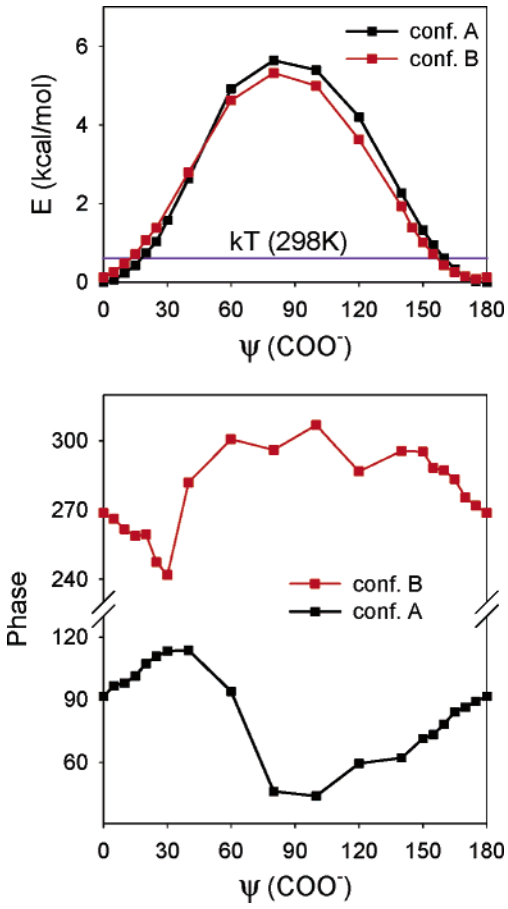

Figure 3. Calculated (B3LYP/6-31++G**/COSMO) dependence of relative molecular energy (top) and the ring phase (bottom) on the rotation of the CO_2^- group. Ring amplitudes remained constant during this motion at 40.2 ± 0.5°.

used. The calculated and experimental intensities agree reasonably well, and most normal modes can be assigned reliably, as summarized in Table 2. Slightly different modes of the deuterated species are assigned in Table 4s in the Supporting Information. Remarkably, the presence of the two conformers in the sample can be clearly manifested as broadening (mode # 6) or even separation (modes 7, 20 (21 for D-Pro)) of a few Raman and ROA bands. Such broadening can also explain some of the relative intensity decrease observed previously in the low-frequency region for Raman and ROA spectra of polyproline.[26] The DFT method provides very good fundamental frequencies on average, with ~5 cm^{-1} of systematic and ~20 cm^{-1} RMS deviations (Tables 2), at least within the far infrared and mid-infrared (IR) range (50−2000 cm^{-1}). Despite this agreement, the detailed comparison of simulated and experimental Raman and ROA spectra in Figure 5 is not completely satisfying. Relative Raman intensities are relatively well reproduced, but the calculated frequencies in the region of C−H and N−H (N−D) bending vibrations (1300−1600 cm^{-1}, modes 28−35) match the experiment rather poorly. We suspect that the influence of anharmonic forces and/or an inadequate description of the solvent interaction with the NH_2^+ group may account for these inconsistencies. The calculated relative ROA intensities (and occasionally the signs) deviate more from the experiment than those for Raman. This can be expected, however, for the second-order differential ROA effect is more sensitive to the adopted approximations. Additionally, for regions of weak and broad

(84) van Mourik, T.; Karamertzanis, P. G.; Price, S. L. *J. Phys. Chem. A* **2006**, *110*, 8−12.
(85) Štrajbl, M.; Florián, J. *Theor. Chem. Acc.* **1998**, *99*, 166−170.

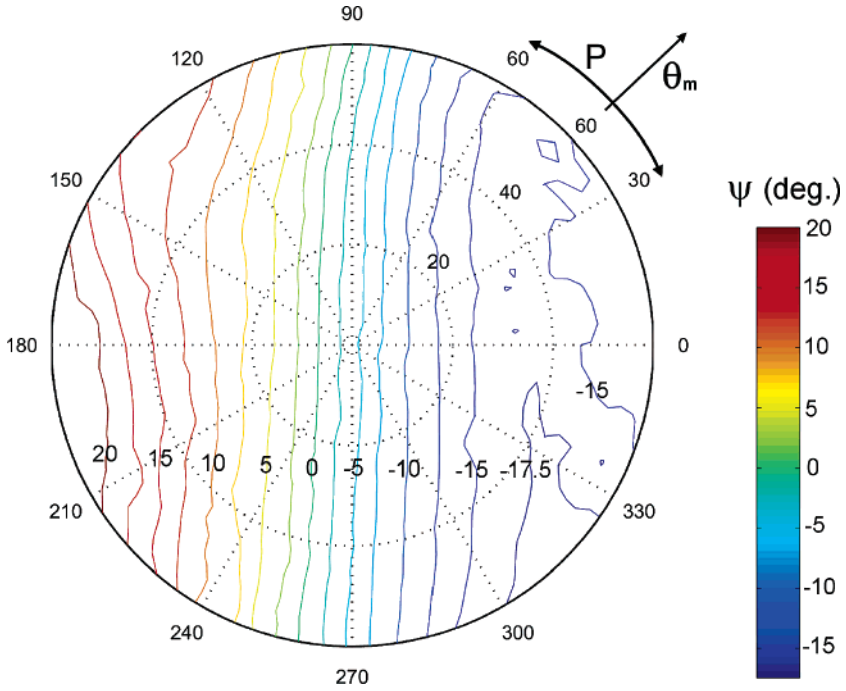

Figure 4. Calculated dependence of the CO_2^- group rotation (ψ) on the proline ring puckering (P, θ_m).

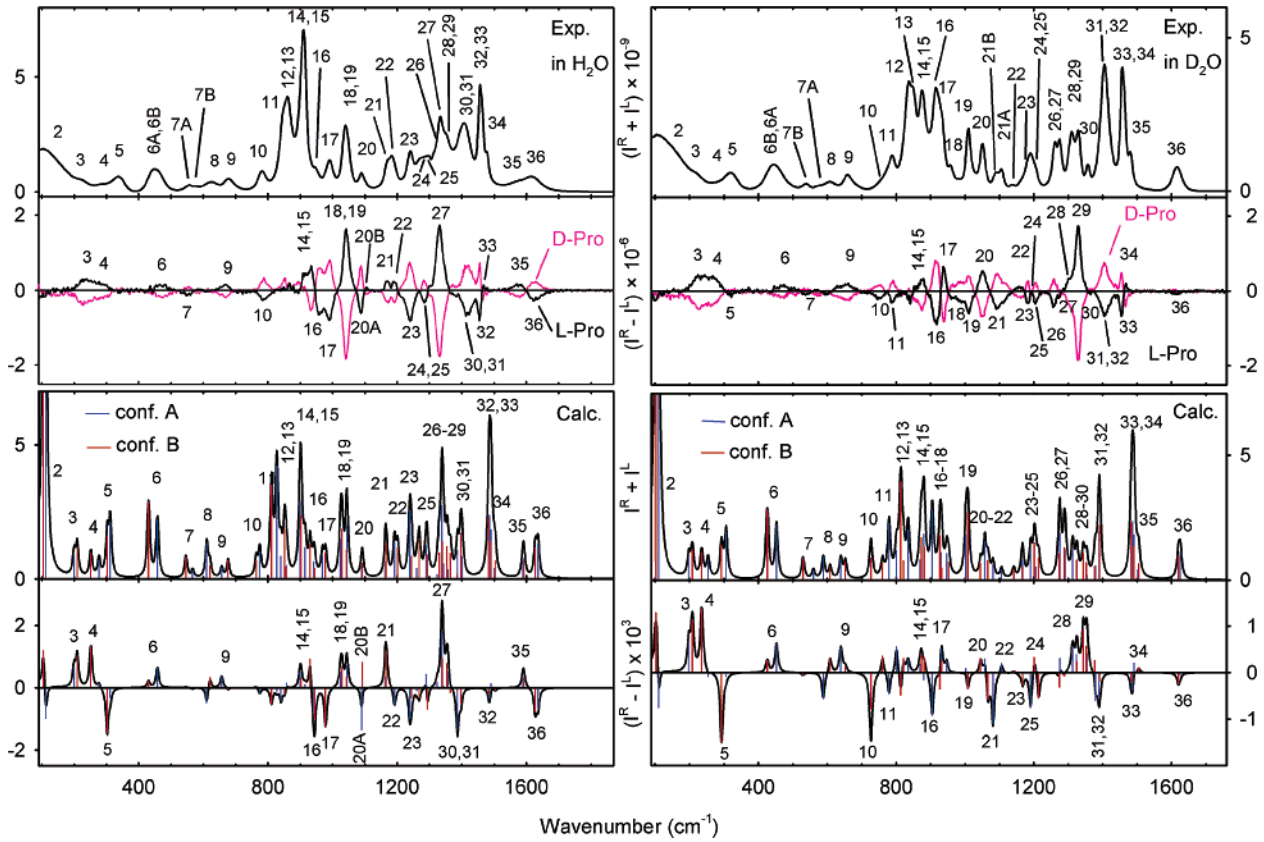

Figure 5. Experimental (top) and calculated (bottom) Raman and ROA spectra of PROZW (left) and deuterated (ND_2) PROZW (right) in aqueous solutions. The calculations (for the L-enantiomers only) were performed at the B3LYP/6-31++G**/COSMO level for both conformers; band positions are marked by the blue and red lines for the **A** and **B** conformers, respectively, and the envelope was obtained as an average.

ROA bands (200−800, 1550−1650 cm^{-1}) the simulation looks significantly less satisfying than that within ∼800−1500 cm^{-1}, where the experimental ROA signal is more structurally intense. However, the influence of molecular dynamics and temperature averaging discussed below partially removes these deficiencies. The intensities (polarizability derivatives) themselves seem to be reproduced with sufficient accuracy with the DFT (B3LYP) method, as the results are comparable with MP2 and HF theories (Figure 4s in SI, also ref 40). Overall, simulated dimensionless circular intensity differences (CIDs, $(I^R - I^L)/(I^R + I^L)$) are in

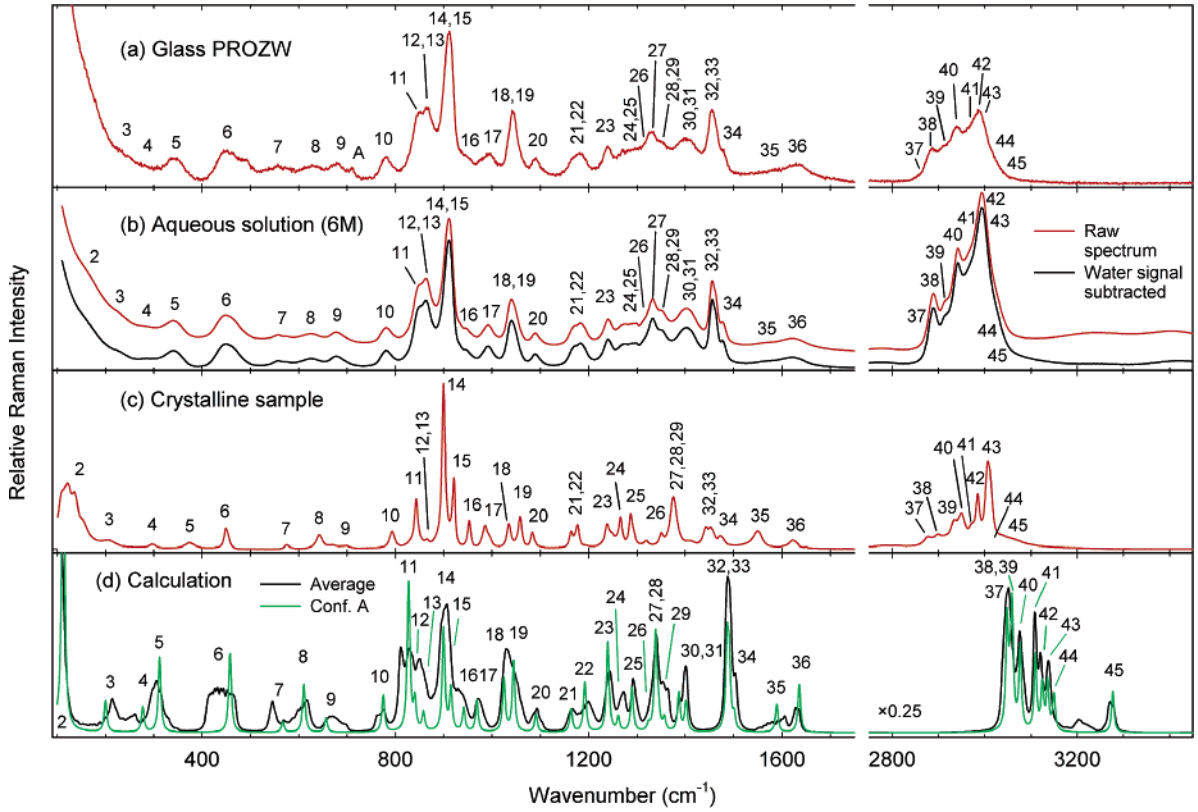

Figure 6. Experimental Raman PROZW spectra obtained for the (a) glass, (b) aqueous solution, and (c) crystal powder with the Raman microspectrometer. The traces in panel d represent spectra calculated at the B3LYP/COSMO/6-31++G** level with (black line, presumably corresponding to the solution) and without (green line) the conformational averaging.

agreement with the experiment (cf. the scales in Figure 5); these are, however, impractical to analyze in detail because of the experimental noise and peak overlapping.

Solution and Solid Raman Spectra. For PROZW in solution we assume that its geometry dispersion approximately corresponds to the energy map and the probability distribution given in Figure 2. On the other hand, in a crystalline sample, the molecular environment is uniform, which restricts also the intramolecular motions, in our case the ring flipping and puckering, especially when this is so coupled with the rotation of the CO_2^- group strongly interacting with the environment. Such a picture is in agreement with the different character of the solution and crystal Raman spectra (Figure 6): the solution bands are much broader, while the powder spectrum is better resolved. Additionally, we can see that the glass spectrum (panel a in Figure 6) is quite close to the solution signal (panel b). A detailed list of the bandwidths obtained by fitting of the experimental bands is given in Table 2. But the glass, as was estimated by integration of the water signal within 3100−3500 cm^{-1}, contains only a negligible amount of water molecules ($\sim$ <2%). Because of the similar dielectric properties of the pure amino acid and water, the zwitterionic form is retained in all the crystal, glass, and solution forms. Thus we explain the similarity of the solution and glass spectra by similar PROZW conformer distributions, largely responsible for the band broadenings.[12] Indeed, only minimal differences (shape of the band of mode 6, an extra band "A" between modes 9 and 10 in panel a, and a wider splitting of the bands 12 and 13 in the glass) are apparent in the glass and solution spectra given in Figure 6. The solution spectrum (panel b in Figure 6) is virtually identical with the Raman spectrum recorded on the ROA spectrometer (Figure 5 for H_2O).

The simulations presented as traces (panel d) in Figure 6 support such an interpretation of the broadening. The Raman spectrum simulated for the equilibrium of conformer **A** (green line) is in reasonably good agreement with the powder spectrum (panel c), namely in terms of bandwidths (a minimal width of 6.5 cm^{-1} was used in the simulations) but also in terms of the overall better frequency agreement (which is apparent, however, only from the detailed statistics of the band frequencies). Regrettably, the simulation fails for the 2800−3300 cm^{-1} anharmonic region. Nevertheless, we can see that after the average over the whole potential energy surface (Figure 2) is taken into account, a very realistic solution/glass spectral shape is obtained for the mid-IR region (Figure 6, black line in panel d). Moreover, the observed selective broadening is reproduced, for example, for the broad signals of modes 6, 21, 22, 35, 36, while some bands remain relatively narrow (modes 14, 17−20, 23, 27, etc.). As was found for the L-alanine zwitterion,[12] the rotation of the CO_2^- group has a large effect on line broadening.

Conformational and Solvent Averaging. For obtaining realistic Raman and ROA spectral shapes both the conformational PROZW motion and the averaging over the positions of the solvent molecules need to be considered. These effects are studied in detail in Figure 7, for the natural (panels a−h) and deuterated (a′−h′) compounds. The 2D puckering averaging (c, d, c′, d′) and the 1D averaging over the CO_2 rotation (e, f, e′, f′), provide very similar spectral shapes. This is understandable because the two motions are so strongly correlated (cf. Figures

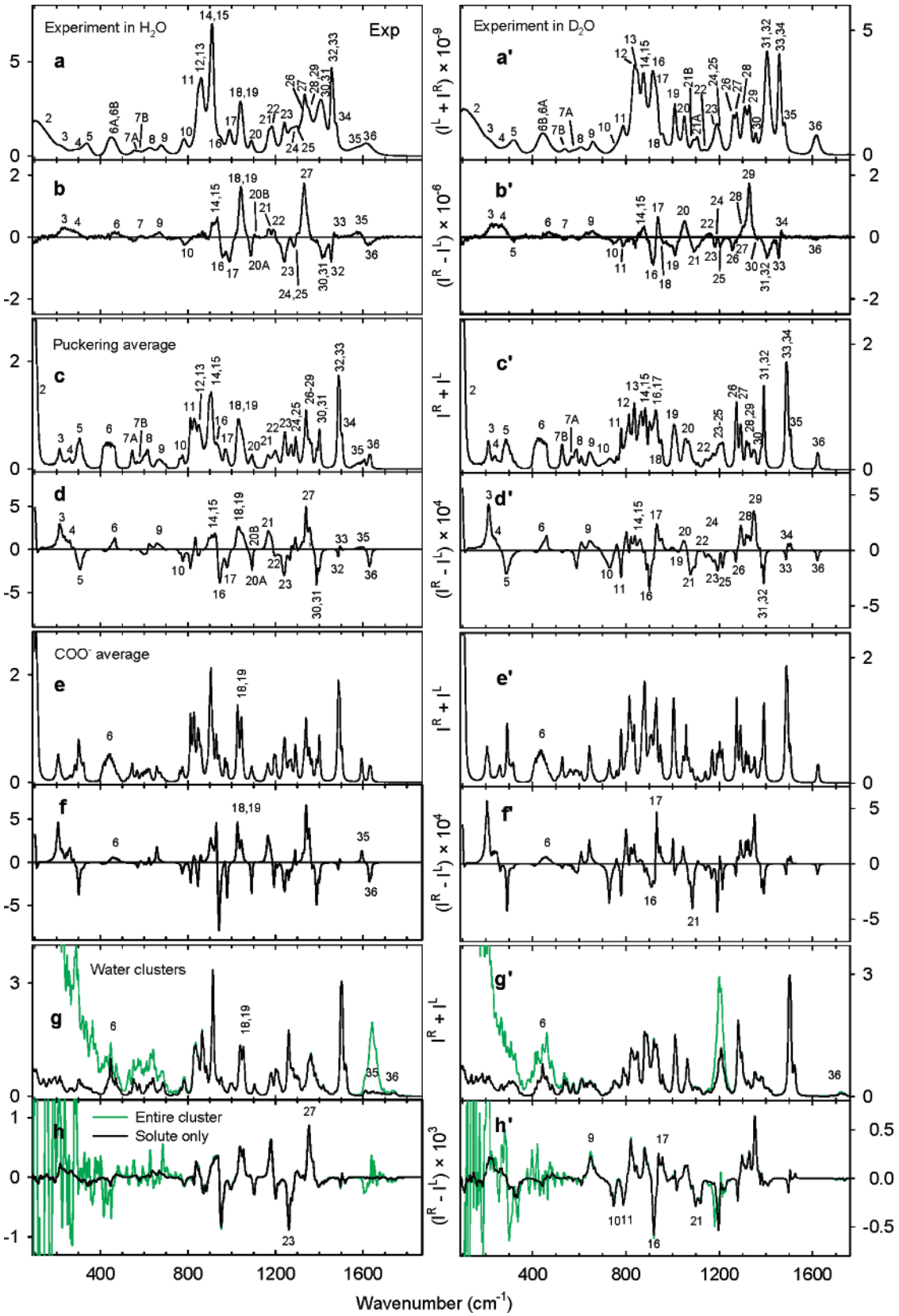

Figure 7. Experimental PROZW (a, b, left) and d2-PROZW (a′, b′, right) Raman and ROA spectra compared to the calculated Boltzmann average (B3LYP/COSMO/6-31++G**) over the puckering (c, d, c′, d′) and CO_2^- rotation (e, f, e′, f ′) for 298 K, and simulated spectra obtained by averaging the signals of 26 explicit PROZW/water clusters (panels g, h, g′, h′).

3, 4). Nevertheless finer differences can be observed, such as the slightly wider peaks, especially for transitions below 1200 cm^{-1}, obtained by the 2D method. The 1D averaging also leads to a more realistic shape of the peak number 6; the puckering average overestimates the band broadening in the region of 400−1200 cm^{-1} but correctly provides the nonsplit peak

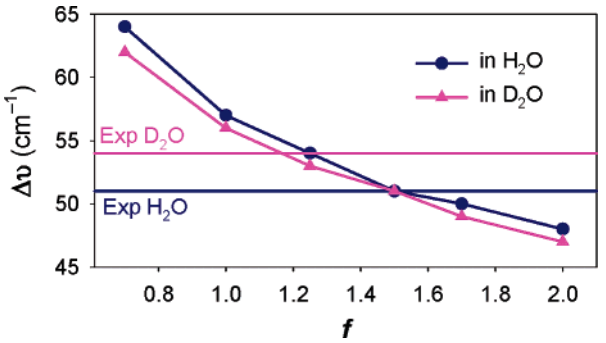

Figure 8. Calculated bandwidth dependence of the CO_2^- out of phase bending band on the PES profile (B3LYP/COSMO/6-31++G** energies were scaled by a uniform factor, $E' = f \times E$).

originating from modes 18 and 19. Thus an ideal model probably lies somewhere between these two approaches. Perhaps a full 3D averaging over the puckering and CO_2^- rotation coordinates would be beneficial, if it were technically feasible. Generally, however, the averaging does improve spectral profiles, if compared to the static two-conformer model (Figure 5). Typically, for both the natural and deuterated species, Raman bands within 200−800 cm^{-1} become broader and less intense, while their shapes become more realistic within 800−1700 cm^{-1} due to the averaging. This is generally also true for the ROA intensities, although relative intensities and occasionally also signs of a few weak bands are not predicted correctly. The vacuum approximation used for the computation of the intensity tensors can account for part of the discrepancies.[86]

It is thus apparent that the experimental spectral profiles cannot be explained fully unless the molecular flexibility is taken into account. Also, vice versa, the Raman and ROA techniques can potentially provide information not only about equilibrium geometries but also about wider areas of the potential energy surface. To investigate the sensitivity of the broadening on PES variation, we simulated the inhomogeneous bandwidth of the asymmetric (out-of-phase) C−C−O bending vibration (found experimentally at ∼450 cm^{-1}) as a function of the conformational barrier. This band is most affected by the broadening and is well separated from other modes. The entire B3LYP/COSMO/6-31++G** PES was scaled arbitrarily ($E' = f \times E$) which modifies the barrier and the potential wells and, as can be seen in Figure 8, is reflected in the bandwidth. Obviously, larger scaling factors (deeper PES minima) lead to narrower widths. Factors of 1.0−1.4 thus provide the best agreement with the experimental broadening and indicate that the computed PES may be quite realistic and close to the true free energy surface of this molecule. The relative difference between the experimental widths for H_2O and D_2O solutions (black and magenta lines in Figure 8) cannot be explained by this model, which suggests that implicit water molecules and their dynamics in the first solvation shell, especially for those hydrogen-bonded to the CO_2^- group, may also contribute to the spectral shape.

In principle, classical molecular dynamics simulations can provide consistently the influence of the solvent and conformational averaging on the spectra. For the *N*-acetylproline amide derivative, very good agreement with experimental IR and VCD spectra was obtained by the MD methods recently.[87] Also, the conformational properties of the proline ring in PROZW and *N*-acetylproline amide appear similar. However, at the current state of theory, we feel that, for Raman spectra simulations where a broader interval of frequencies is needed, the ab initio approach followed in this study is more general, including effects of the charge transfer between the solute and solvent (for the explicit solvent model) that cannot be easily parametrized in MD.

For estimation of the effect of the explicit hydrogen bonding and as an alternative to the COSMO continuum solvent model, the solvent was included in the clusters explicitly. If we go back to Figure 7 we can see the Raman and ROA spectra obtained as averages from 26 PROZW/water clusters (panels g, h, g′, h′). These spectra resemble those computed via the conformational averaging (panels c, d, e, f, c′, d′, e′, *f* ′ in Figure 7 or panel d in Figure 6), in terms of broadening and relative intensity changes of Raman and ROA bands. The analysis is somewhat complicated by the fact that in clusters the effect of the conformation averaging cannot be separated from a "pure" solvent influence. Nevertheless, more realistic spectral profiles in the region 200−800 cm^{-1} are clearly obtained for the clusters. From the raw cluster spectra (green lines in Figure 7) we can suppose that the PROZW vibrations namely below 400 cm^{-1} are strongly coupled with the translational and librational water vibrations,[88] and thus it is conceptually difficult to separate a signal of a pure solute. As could be seen from a visual inspection of the normal modes, for many vibrations water molecules are dragged by the PROZW motion and thus obviously contribute to spectral intensities. For ROA, the average water signal is supposedly close to zero; nevertheless the waters bound to PROZW clearly influence its vibrational activity, improving the sign and intensity patterns namely for modes 6−9. The signal of modes within 800−1600 cm^{-1}, however, presumably interacting less with the aqueous environment, seems to be better predicted by the conformational averaging. For all the approaches, fine frequency splitting of the modes around 1450 cm^{-1} is matched only approximately by our modeling.

Solution−Glass Transition. Finally, in Figure 9, we can observe how the Raman PROZW bands are influenced by the concentration changes. For this molecule, extremely concentrated solutions (6 M) can be made, which leads to minor but clearly visible changes in spectral intensities and frequencies. As can be seen in Figure 9, the solution spectral shapes approximately converge to those of the glass. Moreover, bands assigned to normal mode motions with significant participations of the polar NH_2^+ and CO_2^- groups are influenced most. For example, the frequency of mode number 31, predominantly $^{\alpha}$C−H and N−H bending, changes from 1410 cm^{-1} for the 1 M solution to 1402 cm^{-1} for the 6 M solution, which is close to the maximum of the glass (∼1404 cm^{-1}). The polar molecular parts thus seem to be more sensitive to the environment, while the motion and dynamics of the hydrophobic terminus are influenced less. Due to the relatively small magnitude of the changes and the smooth solution−glass transition, we can still suppose that the ring puckering dynamic and the potential energy surface are similar in both phases. This contrasts with the crystalline state where specific interactions including non-

(86) Pecul, M.; Lamparska, E.; Cappelli, C.; Frediani, L.; Ruud, K. *J. Phys. Chem. A* **2006**, *110*, 2807−2815.
(87) Lee, K. K.; Hahn, S.; Oh, K. I.; Choi, J. S.; Joo, C.; Lee, H.; Han, H.; Cho, M. *J. Chem. Phys. B* **2006**, ASAP.
(88) Bouř, P. *Chem. Phys. Lett.* **2002**, *365*, 82−88.

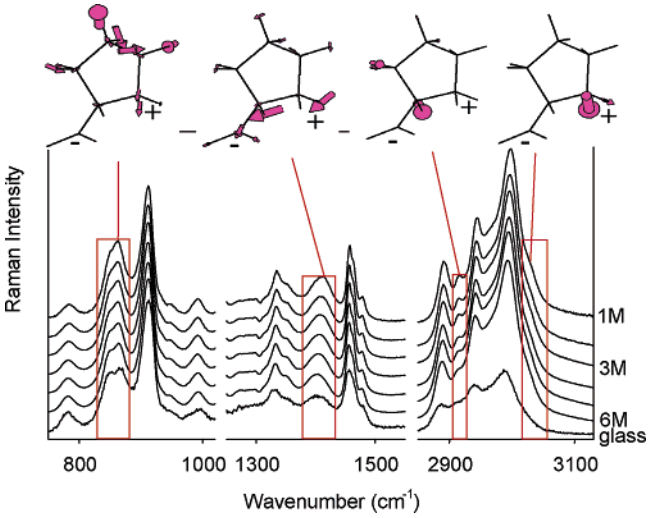

Figure 9. Concentration dependence of the Raman PROZW spectra. Vibrational normal modes that contribute to the most sensitive bands are indicated above. The modes (from left to right) involve ring breathing (ν(C−N)), C−C(O2) stretching, $^{\alpha}$C−H stretching, and N−H stretching.

classical hydrogen bonds were observed.[89] Whether the conformer distribution in the glass is static or whether the molecules can still move freely remains an open question.

Concluding Remarks

For the first time, the proline zwitterion Raman and ROA spectra were interpreted on the basis of ab initio computations. Effects of conformer equilibria, molecular flexibility, temperature averaging, and explicit solvent influence on the spectra could be resolved. The experimental spectra could not be explained and interpreted in full unless the dynamical and solvent factors were involved in the theoretical modeling. The dynamics and environment are of different importance for various spectral bands: some of them are relatively resistant; some are more sensitive to molecular motion, and some, to the coupling with vibrational normal modes of the solvent. The results are consistent with the presence of both conformers in the solution determined also on the basis of NMR spectra analysis. Despite these achievements, we are not entirely satisfied with the results. Fine frequency splitting around 1450 cm^{-1} and in the hydrogen stretching regions could be explained only partially. Deviations still exist between the theoretical and experimental relative intensities, in some cases even ROA signs. Thus future development of the experimental and theoretical methodology is needed so that molecular behavior, dynamics, and interactions in solution can be better understood. On the other hand, improvements of the Raman and ROA optical spectroscopic methods clearly bring more accurate and qualitatively new information about molecular properties. In particular, the advanced interpretational techniques allow monitoring the structure and dynamics of biologically relevant molecules in their native aqueous environment. We find that the behavior of systems as simple as the proline zwitterion is already quite complex but comprehensible on the basis of current methodologies.

Acknowledgment. This work was supported by the Grant Agency (Grant No. 203/06/0420) and by the Ministry of Education of the Czech Republic (MSM 0021620835).

Supporting Information Available: Deuterated PROZW transition assignment, NMR spin−spin coupling constants and proton chemical shifts, computed relative conformer energies, test of DFT integration grids, equilibrium and transition geometries, and one-dimensional sections of the potential energy surface. Comparison of pyrrolidine cation and PROZW potential energy surfaces and comparison of PROZW intensities calculated at MP2, B3LYP, and HF levels. Complete refs 39 and 41 are given. This material is available free of charge via the Internet at http://pubs.acs.org.

JA062958L

(89) Myung, S.; Pink, M.; Baik, M. H.; Clemmer, D. E. *Acta Crystallogr. C* **2005**, *61*, 506−508.